

Synthesis, Improved Antisense Activity and Structural Rationale for the Divergent RNA Affinities of 3'-Fluoro Hexitol Nucleic Acid (FHNA and Ara-FHNA) Modified Oligonucleotides

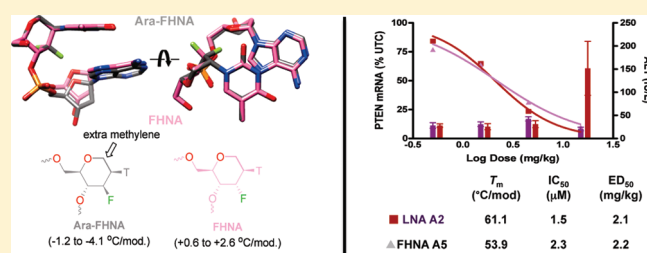
Martin Egli,^{*,†} Pradeep S. Pallan,[†] Charles R. Allerson,^{‡,§} Thazha P. Prakash,[‡] Andres Berdeja,[‡] Jinghua Yu,[‡] Sam Lee,[‡] Andrew Watt,[‡] Hans Gaus,[‡] Balkrishen Bhat,^{‡,§} Eric E. Swayze,[‡] and Punit P. Seth^{*,‡}

[†]Department of Biochemistry, School of Medicine, Vanderbilt University, 607 Light Hall, Nashville, Tennessee 37232, United States

[‡]Isis Pharmaceuticals Inc., 1891 Rutherford Road, Carlsbad, California 92008, United States

S Supporting Information

ABSTRACT: The synthesis, biophysical, structural, and biological properties of both isomers of 3'-fluoro hexitol nucleic acid (FHNA and Ara-FHNA) modified oligonucleotides are reported. Synthesis of the FHNA and Ara-FHNA thymine phosphoramidites was efficiently accomplished starting from known sugar precursors. Optimal RNA affinities were observed with a 3'-fluorine atom and nucleobase in a *trans*-diaxial orientation. The Ara-FHNA analog with an equatorial fluorine was found to be destabilizing. However, the magnitude of destabilization was sequence-dependent. Thus, the loss of stability is sharply reduced when Ara-FHNA residues were inserted at pyrimidine-purine (Py-Pu) steps compared to placement within a stretch of pyrimidines (Py-Py). Crystal structures of A-type DNA duplexes modified with either the monomer provide a rationalization for the opposing stability effects and point to a steric origin of the destabilization caused by the Ara-FHNA analog. The sequence dependent effect can be explained by the formation of an internucleotide C—F···H—C pseudo hydrogen bond between F3' of Ara-FHNA and C8—H of the nucleobase from the 3'-adjacent adenosine that is absent at Py-Py steps. In animal experiments, FHNA-modified antisense oligonucleotides formulated in saline showed a potent downregulation of gene expression in liver tissue without producing hepatotoxicity. Our data establish FHNA as a useful modification for antisense therapeutics and also confirm the stabilizing influence of F(Py)···H—C(Pu) pseudo hydrogen bonds in nucleic acid structures.



INTRODUCTION

Antisense oligonucleotides (ASOs) bind to their cognate mRNA by Watson–Crick base pairing and modulate mRNA function.¹ Over the past decade, interest in antisense technology has grown exponentially with the discovery of siRNA and miRNA based mechanisms for modulating gene expression² and by the realization that RNA plays a far more important role in cell biology than serving just as a conduit for the transfer of genetic information.³ In addition, second generation ASOs that downregulate gene expression by employing an RNase H mechanism have shown robust antisense pharmacology in humans and established nucleic acid based therapeutics as a viable drug discovery platform.⁴

As part of a comprehensive effort aimed at understanding the structure–activity relationship (SAR) of ASOs containing high affinity modifications, with the aim of advancing a new oligonucleotide modification toward human trials, we recently compared the antisense properties of locked nucleic acid (LNA, 13) and related analogs such as 2',4'-constrained 2'-O-Et (cEt, 14) (Figure 1).^{5–8} As an extension of that work, we evaluated the *in vivo* properties of the hexitol class of oligonucleotide modifications that are also known to increase affinity for cognate

RNA.⁹ In the hexitol series, the furanose ring found in DNA 1 and RNA 2 is replaced with a six-membered pyranose ring and the position of the nucleobase is moved from the anomeric carbon to the 2'-position (Figure 1). This arrangement positions the nucleobase in an axial orientation and mimics the N-type sugar pucker of furanose nucleosides.

The Herdewijn group described the synthesis, biophysical, structural, and preliminary biological characterization of HNA (hexitol nucleic acid, 7), ANA (altritol nucleic acid, 8), 3'-O-Me ANA 9, and MNA (mannitol nucleic acid, 10) modified oligonucleotides.⁹ However and much to our surprise, the 3'-fluoro hexitol derivative (FHNA, 11) and its “arabino” analog (Ara-FHNA, 12) have not been described to date. Given the usefulness of the 2'-fluoro modification (FRNA, 5) in siRNA,^{10,11} miRNA,¹² and aptamer¹³ based oligonucleotide therapeutic applications and the general importance of fluorine as a “polar hydrophobic” substituent in medicinal chemistry,¹⁴ we were intrigued by the potential of FHNA as a modification for antisense therapeutics. As well we were keen on assessing Ara-FHNA

Received: July 28, 2011

Published: September 14, 2011

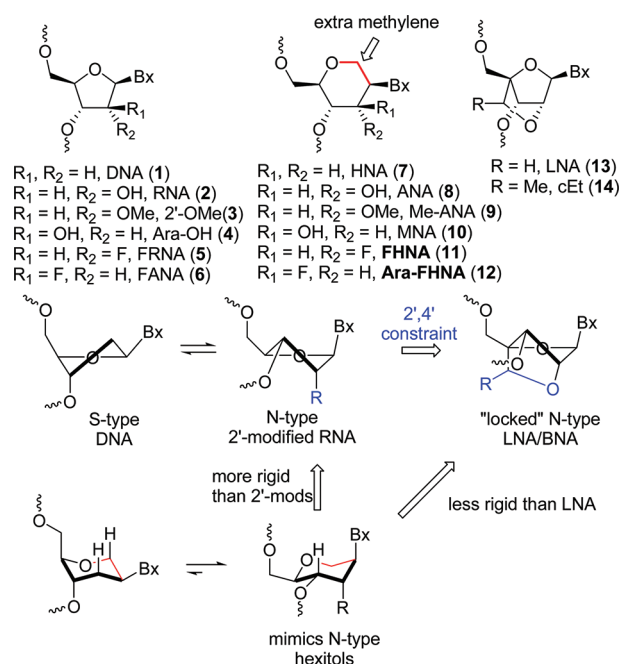
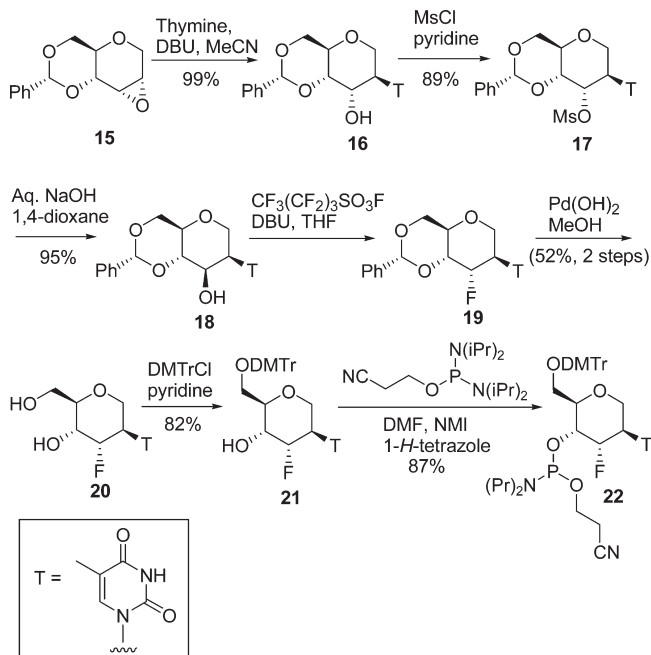


Figure 1. Structural relationships between 2'-modified RNA, hexitol, and 2',4'-bridged nucleic acids.

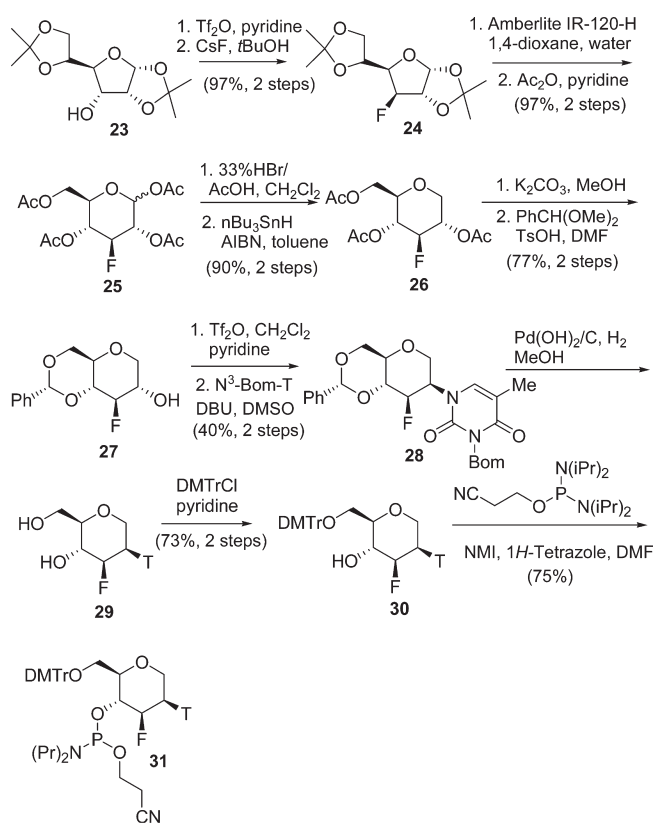
Scheme 1. Synthesis of FHNA Thymine Phosphoramidite



because the 2'-fluoroarabino modification (FANA, 6) displayed increased RNA affinity relative to DNA and was found to be one of only a handful of analogs that elicits cleavage of the targeted RNA strand by RNase H.¹⁵

In this manuscript, we describe the synthesis, biophysical, structural, and biological properties of oligo-2'-deoxyribonucleotides modified with one or more FHNA and Ara-FHNA monomers. Whereas axial 3'-fluoro substitution (FHNA) boosts the RNA affinity of HNA, fluorine in the equatorial orientation

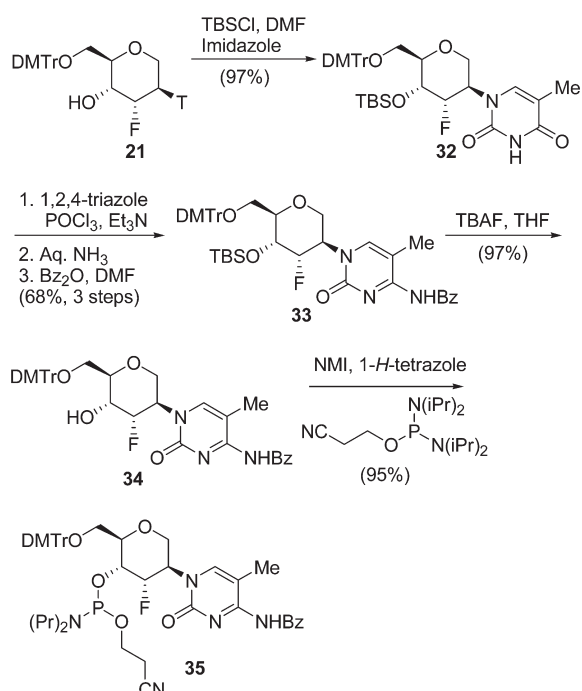
Scheme 2. Synthesis of Ara-FHNA Thymine Phosphoramidite



(Ara-FHNA) results in a significant destabilization relative to both HNA and DNA. Thus, the consequences of 3'-fluoro substitution of HNA differ distinctly from those of 2'-fluoro substitution of DNA (FRNA and FANA), in that both latter analogs exhibit increased RNA affinity relative to the parent oligomer. Subsequently, we conducted a detailed crystallographic analysis of FHNA-, Ara-FHNA-, FRNA- and FANA-modified oligo-2'-deoxynucleotides that provides insight into the structural origins of the initially surprising observations with regard to the relative pairing affinities.

RESULTS

Synthesis of FHNA and Ara-FHNA Pyrimidine Nucleoside Phosphoramidites. Synthesis of FHNA pyrimidine nucleoside phosphoramidites was accomplished as shown in Scheme 1. Treatment of known epoxide 15 with thymine in the presence of DBU provided the corresponding hexitol nucleoside 16.^{16,17} Mesylation of the secondary hydroxyl group provided mesylate 17 which was treated with aqueous sodium hydroxide to provide the "ara" nucleoside 18 via formation and opening of the anhydro-nucleoside intermediate as described previously.¹⁸ Treatment of nucleoside 18 with nonafluorobutanesulfonyl fluoride and DBU provided the fluorinated nucleoside 19 via S_N2 inversion of the 3'-hydroxyl group,^{19,20} which was typically contaminated with 5–10% of a byproduct arising from elimination of the nonaflate intermediate. It was difficult to completely remove the elimination byproduct from the fluorinated nucleosides at this stage by silica gel chromatography. Instead the partially purified mixture was hydrogenated using palladium

Scheme 3. Synthesis of FHNA 5-Methylcytosine Phosphoramidite


hydroxide on carbon to provide the deprotected nucleoside **20**, which could now be conveniently purified by chromatography. While the overall yield for the fluorination/benzylidene removal was $\sim 50\%$ for the two step process, this procedure could be used conveniently for the preparation of **20** on a multigram scale. The 6'-hydroxyl group was then protected with dimethoxytrityl chloride to provide nucleoside **21**, which was converted to the desired phosphoramidite **22** by means of a phosphitylation reaction.

For synthesis of Ara-FHNA phosphoramidite **31**, all methods to carry out direct fluorination of nucleoside **16** were unsuccessful due to competing formation of the anhydro-nucleoside via attack of O-2 of the pyrimidine ring on the leaving group generated by activation of the 3'-hydroxyl group. To circumvent these problems, we carried out the fluorination on diacetone allofuranose **23** to install the problematic fluorine atom early in the synthesis (Scheme 2). Fluorination was accomplished by first conversion of the 3'-hydroxyl group in **23** to the corresponding triflate followed by displacement with cesium fluoride in *t*-BuOH²¹ to provide **24** in essentially quantitative yield. Treatment of **24** with an acidic resin under aqueous conditions resulted in hydrolysis of both acetonide protecting groups and rearrangement to the more stable pyranose ring structure which was per-acetylated to provide fluoro sugar **25** as an anomeric mixture.^{22,23} Conversion of the anomeric acetates to the anomeric bromide using HBr/acetic acid followed by reduction using $n\text{Bu}_3\text{SnH/AIBN}$ provided the fluoro hexitol sugar **26**.²⁴ Removal of the acetate protecting groups followed by re-protection of the 4'- and 6'-hydroxyl groups as the cyclic benzylidene furnished the protected hexitol intermediate **27**. Synthesis of the N^3 -Bom protected thymine nucleoside **28** was accomplished by first conversion of the 2'-hydroxyl group in **27** to the triflate followed by displacement with N^3 -Bom protected thymine. It was necessary to use the protected nucleobase to prevent competing

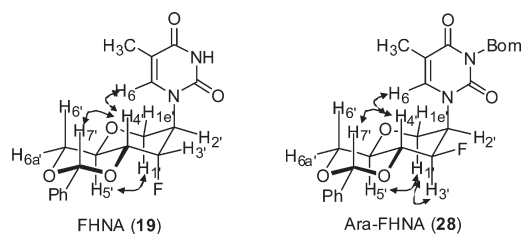


Figure 2. Structural determination of FHNA and Ara-FHNA nucleosides showing key NOESY crosspeaks.

displacement of the triflate by N^3 of thymine. The formation of **28** was also accompanied with the formation of a separable byproduct ($\sim 20\%$) arising from displacement of the sugar triflate by O-2 of N^3 -Bom thymine. As our motivation at this point was to prepare enough material to complete our initial evaluation of Ara-FHNA in T_m studies, we did not attempt to optimize the nucleoside formation reaction any further. Removal of the N^3 -Bom group and the 4,6-O-benzylidene was accomplished by catalytic hydrogenation using 20% palladium hydroxide on carbon to provide the Ara-FHNA thymine nucleoside **29**, which was not purified but directly converted to the 6'-O-DMTr ether **30**. A phosphitylation reaction provided the desired phosphoramidite **31**.

The 5-methylcytosine FHNA phosphoramidite **35** was synthesized according to the procedure outlined in Scheme 3. The 4'-hydroxyl group in **21** was first protected as the *tert*-butyldimethylsilyl ether to provide **32** in excellent yield. The thymine nucleobase was next converted to the 4-*N*-benzoyl protected 5-Methylcytosine nucleobase by a three-step sequence.²⁵ Reaction of **32** with POCl_3 followed by displacement of the 4-chloro intermediate with 1,2,4-triazole provided the corresponding triazolide which was further displaced with aqueous ammonia to provide the 5-methylcytosine nucleoside. The crude nucleoside was dried and the exocyclic amino group on the heterocycle was reacted with benzoic anhydride to provide the 4-*N*-benzoyl protected nucleoside **33** in good yield (68% over three steps). The 4'-O-TBS group in **33** was removed using TBAF to provide **34** followed by a phosphitylation reaction to provide the desired phosphoramidite **35**. All the hexitol phosphoramidites were incorporated into oligonucleotides using standard automated phosphoramidite chemistry using procedures described previously.²⁵

The relative orientation of the fluorine atom in FHNA and Ara-FHNA nucleosides was assigned by examination of the fluorine-proton coupling constants in nucleosides **19** and **28** and by NOESY spectroscopy (Figure 2). In the case of FHNA nucleoside **19**, the axial fluorine atom showed a large geminal coupling ($J_{\text{F,H}3'} = 47.8$ Hz) to $\text{H}3'$, another large *trans*-diaxial coupling to $\text{H}4'$ ($J_{\text{F,H}4'} = 29.8$ Hz), and a smaller (axial/equatorial) coupling to $\text{H}2'$ ($J_{\text{F,H}2'} = 8.0$ Hz). In turn, $\text{H}3'$ showed a large coupling to the geminal fluorine ($J_{\text{H}3',\text{F}} = 48.2$ Hz) and small couplings (< 3 Hz) to $\text{H}2'$ and $\text{H}4'$. In contrast, in nucleoside **28**, the equatorial fluorine showed a large geminal coupling to $\text{H}3'$ ($J_{\text{F,H}3'} = 48.2$ Hz), intermediate (equatorial/axial) coupling to $\text{H}4'$ ($J_{\text{F,H}4'} = 10.3$ Hz), and a long-range coupling to $\text{H}1\text{e}'$ ($J_{\text{F,H}1\text{e}'} = 5$ Hz). In addition, $\text{H}3'$ showed a large geminal coupling to fluorine ($J_{\text{H}3',\text{F}} = 48.2$ Hz), a large *trans*-diaxial coupling to $\text{H}4'$ ($J_{\text{H}3',\text{H}4'} = 9.8$ Hz), and a smaller (axial/equatorial) coupling to $\text{H}2'$ ($J_{\text{H}3',\text{H}2'} = 6.2$ Hz). NOESY crosspeaks were visible between $\text{H}4'$ and the pyrimidine $\text{H}6$ for both

Table 1. Characterization of FHNA, Ara-FHNA, HNA, and LNA Analogs Based on T_m Values for DNA Sequences Containing One, Two, or Three Modified Nucleotides

Sequence ^a (5' to 3')	ΔT_m /modification (°C) ^b				
	DNA	FHNA	Ara-FHNA	HNA	LNA
GCGTtTTTGCT	(45.6)	+0.6	-2.8	+0.5	+5.2
GCGTtTTTGCT	(45.6)	+1.7	-4.1	+0.9	+4.7
CCAGtGAtAtGC	(42.6)	+2.6	-1.2	+1.4	+6.7

^a Uppercase letters indicate 2'-deoxynucleotides; bold lower case letters indicate modified nucleotides. ^b T_m values were measured at 4 μ M oligo concentration in 10 mM sodium phosphate buffer (pH 7.2) containing 100 mM NaCl and 0.1 mM EDTA; the sequences of the RNA complements were 5'-r(AGCAAAAACGC)-3' and 5'-r(GCAUAU-CACUGG)-3'; T_m values reflect the average of at least three individual measurements with a standard deviation of ≤ 0.27 °C.

Table 2. Mismatch Discrimination Properties of FHNA

Modification	T_m ($\Delta T_m = T_m(\text{mismatch}) - T_m(\text{match})$) (°C) ^{a,b}			
	X = A	X = G	X = C	X = T
DNA	45.6	41.5 (-4.1)	32.4 (-13.4)	31.9 (-13.7)
FHNA	46.2	36.3 (-9.9)	34.3 (-11.9)	38.9 (-7.3)
LNA	50.8	45.6 (-5.2)	34.1 (-16.7)	37.2 (-13.6)

^a Sequence used for evaluation of 5'-d(GCGTtTTTGCT)-3' where the bold letter indicates the modified nucleotide. ^b Sequence of RNA complement 5'-r(AGCAAAAACGC)-3' where X indicates the mismatch site.

19 and **28** establishing the axial orientation of the nucleobase. In addition, for **28**, NOESY crosspeaks were visible between H3', H1', and HS', while NOESY crosspeaks were only visible between H1' and HS' for **19**.

FHNA and Ara-FHNA Show Opposite Trends in Affinity for Complementary RNA. We first evaluated the thermal stability (T_m) of FHNA and Ara-FHNA modified duplexes using single, double, and triple incorporations of the modified nucleotide and compared them to LNA and HNA modified duplexes (Table 1). FHNA exhibited slightly improved T_m as compared to HNA, but the magnitude of stabilization was significantly less than that observed for LNA modified duplexes. Interestingly, we observed higher duplex stabilization when FHNA T was incorporated in tandem or between A or G as compared to incorporation in a stretch of dTs. In contrast, Ara-FHNA was destabilizing. The duplex destabilization observed with Ara-FHNA is somewhat unexpected as the corresponding furanose analog, FANA **6**, improves the thermal stability of oligonucleotide duplexes by formation of a pseudo H-bond at pyrimidine/purine steps.²⁶

However, the result is consistent with the binding properties reported for MNA **10** which has an equatorial hydroxyl group at the 3'-position.²⁷ Remarkably, when three Ara-FHNA-Ts were incorporated before A or G, the loss in stability was considerably diminished compared to sequences with either one or two modifications in a stretch of dTs (Table 1). For now we note that there appears to be a sequence-dependent effect on the stability as a result of the Ara-FHNA modification.

Mismatch Discrimination and Nuclease Resistance Properties of FHNA Modified Oligonucleotides. We also

Table 3. 3'-Exonuclease Stability of the Phosphodiester Linkage in DNA, MOE, LNA, FHNA, and Ara-FHNA Modified Oligonucleotides

Sequence (5'-3')	Modification ^a	$T_{1/2}$ (min) ^b
TTTTTTTTTTTT	DNA	0.23
TTTTTTTTTTTTt	MOE	3
TTTTTTTTTTTTt	LNA	3
TTTTTTTTTTTTt	FHNA	160
TTTTTTTTTTTTt	Ara-FHNA	101

^a Uppercase letters indicate 2'-deoxynucleotides, bold letters indicate modified nucleotides, and MOE indicates 2'-O-methoxyethyl ribose modification. ^b Each oligonucleotide was prepared as a 500 μ L mixture containing the following: 12.5 μ L of 200 μ M oligomer, 50 μ L of SVDP at 0.005 Units/mL in SVDP buffer (50 mM Tris-HCl, pH 7.5, 8 mM MgCl₂) final concentration 0.0005 Units/mL, 438.5 μ L of SVP buffer. Samples were incubated at 37 °C in a thermoblock. Aliquots (50 μ L) were taken at different intervals. EDTA was added to aliquots immediately after removal to quench enzyme activity, and the samples were analyzed on IP HPLC/MS. The results are expressed as half-life ($T_{1/2}$) in minutes.

characterized the mismatch discrimination and nuclease resistance properties of FHNA oligonucleotides. In the mismatch experiments, FHNA showed substantially better discrimination for the G-T wobble base pair but diminished recognition of the T-T mismatched pair relative to DNA and LNA (Table 2). Both the FHNA- and the Ara-FHNA-modified DNAs also exhibited much higher resistance to exonuclease digestion as compared to LNA- and MOE-modified oligonucleotides (Table 3).

X-ray Crystallography of Oligonucleotides Containing FHNA-T or Ara-FHNA-T Modifications. To gain insight into the origins of the divergent hybridization behaviors of the FHNA and Ara-FHNA modifications, we determined crystal structures of DNA decamer duplexes [d(GCGTAtACGC)]₂ containing either FHNA-T or Ara-FHNA-T (**t6** and **t16**; nucleotides in the paired strands are numbered 1–10 and 11–20) at resolutions of 1.56 and 1.67 Å, respectively. Selected crystal data, data collection, and refinement parameters are listed in the Supporting Information (Table S2) along with examples of the quality of the final electron density (Figure S1). The decamers adopt A-form geometry, and their overall conformations are similar (Supporting Information, Figure S2). Visual inspection of the structures and the analysis of helical parameters²⁸ and the sugar-backbone geometry demonstrate that FHNA and Ara-FHNA residues fit well into the oligo-2'-deoxynucleotide duplex. Thus, there are no kinks associated with the sites of incorporation of modified residues as judged by the curvature of the helical axis and local rolling of base pairs. The average values for helical rise and twist are 2.93 Å and 31.8°, respectively, in the FHNA-modified duplex, and they are 2.86 Å and 32.1°, respectively, in the Ara-FHNA-modified duplex. Among the global base-axis parameters, both X-displacement (-4.3 Å, FHNA; -4.6 Å, Ara-FHNA) and inclination (5.6°, FHNA; 8.6°, Ara-FHNA) are slightly higher in the Ara-FHNA-modified duplex. The sugars of all 2'-deoxynucleotides adopt the C3'-endo pucker. In both duplexes, residue A5 displays a so-called extended variant of the backbone with torsion angles α and γ both in the *ap* range instead of the standard *sc*- and *sc*+ conformations respectively. In the FHNA-modified duplex, G13 also adopts an extended backbone. However, the six backbone torsion angles and the glycosidic angles of all FHNA and Ara-FHNA nucleotides **t6** and **t16** fall into the standard ranges.

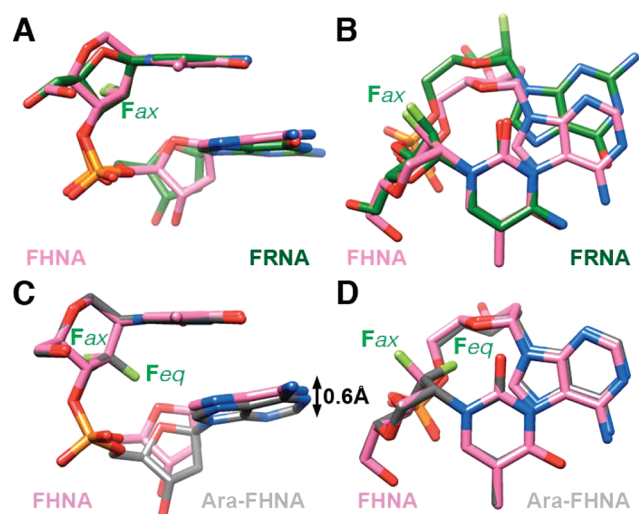


Figure 3. Comparison between the conformations of dinucleotides containing the FHNA (fh; pink carbons), Ara-FHNA (afh; gray carbons), or FRNA (fr; green carbons) modifications. Superimposition of fh(T)pd(A) and fr(C)pfr(G),¹¹ (A) viewed into the major groove and (B) rotated by 90° and viewed perpendicularly to the thymine plane. Superimposition of fh(T)pd(A) and afh(T)pd(A), (C) viewed into the major groove, revealing slight unstacking of bases in the case of Ara-FHNA (double arrow), and (D) rotated by 90° and viewed perpendicularly to the thymine plane. Nitrogen, oxygen, and phosphorus atoms are colored blue, red, and orange, respectively, and axial 2'- and axial or equatorial 3'-fluorine atoms are highlighted in light green and are labeled.

We take the similar overall geometries of the two duplexes as evidence that putative deviations at the local level between the two structures, at the sites of either FHNA or Ara-FHNA incorporation, can be attributed to the particular steric and stereoelectronic characteristics of the two modifications. In the following paragraphs we analyze the conformational features of the base-pair steps containing FHNA and Ara-FHNA modifications. We compare them to base-pair steps in A-form duplexes featuring the corresponding furanose analogs, FRNA and FANA, respectively, which we have previously analyzed in considerable detail in terms of their conformational preferences,^{11,29} and correlate the stability data (Table 1) with the structural observations.

The axial fluorine atom in FHNA juts out into the minor groove in a direction that is virtually perpendicular to the trajectory of the backbone, and this precludes short contacts between the 3'-substituent and backbone and/or base atoms of the 3'-adjacent nucleotide (dA7 in strand 1 and dA17 in strand 2; Figure 3A,B). The spacing between adjacent bases in FHNA and FRNA are very similar, and the only difference is a slight shift of adenine into the major groove in the FHNA-modified structure relative to the corresponding FRNA base. We used FRNA as a reference here because FRNA and RNA adopt virtually identical structures.¹¹ Moreover, rather than a difference between the TpA (FHNA) and CpG (FRNA) steps in the A-form settings compared here, the slight offset in the positions of the nucleobases is most likely a consequence of the geometric constraints of the furanose and hexose sugars.

In contrast to the axial fluorine in FHNA, modeling an equatorial 3'-fluorine into the structure of the FHNA-modified duplex leads to several short contacts between fluorine and atoms from the 3'-adjacent nucleotide (Supporting Information, Figure S3).

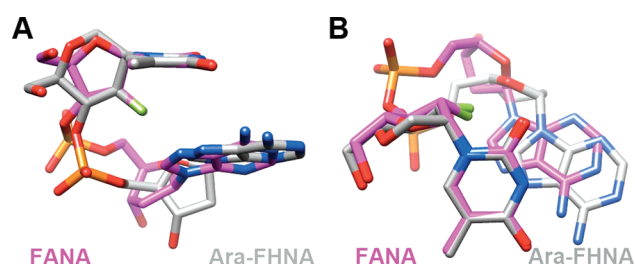


Figure 4. Comparison between the conformations of dinucleotides containing the Ara-FHNA (afh; gray carbons) or FANA (fa; magenta carbons) modifications. Superimposition of afh(T)pd(A) and fa(T)pd(A),²⁹ (A) viewed into the major groove and (B) rotated by 90° and viewed perpendicularly to the thymine plane. Please see Figure 3 for color codes of individual atoms.

In this hypothetical model, the shortest among these distances is between F3'(t6) and O4'(dA7): 2.19 Å. Even considering a van der Waals radius for fluorine of 1.2 Å (matching that of H), such a contact would be strongly destabilizing. Therefore, in order to accommodate the Ara-FHNA residue, one would expect the dinucleotide step to undergo a conformational change.

Indeed, the superimposition of dinucleotides containing either FHNA-T or Ara-FHNA-T followed by 2'-deoxy-A reveals that the latter residue is pushed away in the Ara-FHNA-modified decamer duplex (Figure 3A,C). The resulting internucleotide distances between the equatorial fluorine and the 4'-oxygen in the two strands of 2.75 Å (F3'[t6]...O4'[dA7]) and 2.82 Å (F3'[t16]...O4'[dA17]) correspond to the sum of the van der Waals radii. However, avoiding a steric clash causes partial unstacking of the adenine from Ara-FHNA-T (Figure 3C,D), which likely contributes to the unfavorable RNA affinity observed for Ara-FHNA relative to FHNA, HNA, and DNA (Table 1).

Unlike in the case of HNA, addition of a fluorine in the arabino configuration to 2'-deoxyribose (FANA 6, Figure 1) has a positive effect on the RNA affinity, whereby the stability increase is highest at pyrimidine-purine steps due to formation of an F2'(Py)...H-C8(Pu) pseudo hydrogen bond.²⁶ FANA-T (t) incorporated into the A-form decamer d(CGCTAtACGC) was found to be unable to adopt a pure C3'-endo pucker.²⁹ Moreover, it forces the 3'-adjacent deoxyribose into a C2'-endo pucker (Supporting Information, Figure S4). The resulting dinucleotide step exhibits a considerable roll and F2'(FANA-T)...C8(dA) contacts as short as 2.55 Å.²⁹ A comparison between the conformation of dinucleotides containing either a 5'-Ara-FHNA-T or a -FANA-T demonstrates different degrees of rolling and a larger slide of the adenine moiety following the Ara-FHNA nucleotide (Figure 4). The latter is a consequence of the steric constraints of the HNA framework and the equatorial 3'-fluorine that pushes away the adjacent sugar. These constraints preclude tight F3'(Ara-FHNA-T)...C8(dA) contacts such as those in the FANA-modified duplex (Figure 4 and Supporting Information, Figure S4). Nevertheless, the resultant distances of 3.09 and 3.12 Å in strands 1 and 2, respectively, of the Ara-FHNA-modified duplex appear still sufficient to offset the loss of stability due to diminished stacking (Figure 3C), so as to merely reduce the T_m by 1.2 °C/modification for multiple incorporations at pyrimidine-purine steps (Table 1).

Biological Evaluation of FHNA Modified Antisense Oligonucleotides. We next evaluated FHNA A1, HNA A2, and LNA

A3 ASOs in T_m , cell culture, and a single dose escalation experiment in mice using a 14-mer oligonucleotide sequence targeting mouse phosphatase and tensin homologue (PTEN) mRNA (Table 4, Figure 5A,B). In T_m measurements we measured duplex thermal stability versus the length matched 14-mer and a longer 20-mer RNA complement. We used the 20-mer complement since the biological receptor (i.e., mRNA) for these ASOs is not length matched to the ASO. When the T_m was measured versus the 14-mer RNA complement, both the hexitol ASOs **A1** and **A2** exhibited similar duplex thermal stabilities which were substantially lower than that of LNA ASO **A3**.

Table 4. T_m in Vitro and in Vivo activity of FHNA, HNA, and LNA gapmer ASOs targeting mouse PTEN mRNA

ASO ^a	T_m (°C) ^b vs 14-mer RNA	T_m (°C) ^c vs 20-mer RNA	IC ₅₀ (μM) ^d	ED ₅₀ (mg/kg) ^e	ED ₅₀ (mg/kg) ^f
FHNA A1	53.9	60.1	2.3	7.8	2.2
HNA A2	54.9	58.0	2.4	13.8	NT
LNA A3	61.1	65.4	1.5	7.2	2.1

^aSequence used for evaluation of ^mCTTAGCACTGGC^mCT; bold letters indicate modified residues in flanks, and uppercase letters indicate 2'-deoxynucleotides in the gap; all linkages are phosphorothioate modified. ^bSequence of 14-mer RNA complement 5'-r(AGGCCAG-UGCUAAG)-3'. ^cSequence of 20-mer RNA complement 5'-r(UCAAGGCCAGUGCUAAGAGU)-3'. ^dIC₅₀ for PTEN mRNA reduction in mouse bEND cells with electroporation. ^ePotency for PTEN mRNA reduction in mouse liver from single dose study. ^fPotency for PTEN mRNA reduction in mouse liver from 3-week study.

However, all the ASOs exhibited improved duplex thermal stabilities when the T_m was measured using the longer 20-mer complement. Presumably, the overhanging nucleotides improve duplex thermostability by providing additional stacking interactions with the modified nucleotides in the flanks of the ASO.³⁰ However, these interactions appear to be somewhat more important for FHNA (ΔT_m 20-mer-14-mer +6.2 °C) as compared to HNA (ΔT_m +3.1 °C) and LNA (ΔT_m +4.3 °C) oligonucleotides.

In cell culture, FHNA ASO **A1** and HNA ASO **A2** exhibited similar potency for downregulating PTEN mRNA but both ASOs were slightly less potent than LNA ASO **A3** (Table 4 and Figure S6). In the animal experiment, mice were injected i.p. with a single dose of 3.2, 10, 32, and 100 mg/kg of ASOs **A1**, **A2**, and **A3** in saline and liver PTEN mRNA and plasma alanine amino transferase (ALT) levels were measured postsacrifice. In this experiment, the FHNA ASO **A1** exhibited near identical potency as the LNA ASO **A3** while the HNA ASO **A2** was 2-fold less potent. However, there was a dramatic difference in the markers for hepatotoxicity for these ASOs. The LNA ASO **A3** showed ALT increases for the high dose group treated animals while the hexitol ASOs did not. To determine if the improved activity of FHNA was because of improved biodistribution, we measured tissue levels of all three ASOs in mouse liver (Supporting Information, Figure S5). Both FHNA and LNA ASOs showed comparable tissue accumulation at all doses except for the high dose group where the LNA ASO levels were higher. The HNA ASO showed slightly lower tissue accumulation at all the doses tested. In a subsequent experiment, we evaluated the

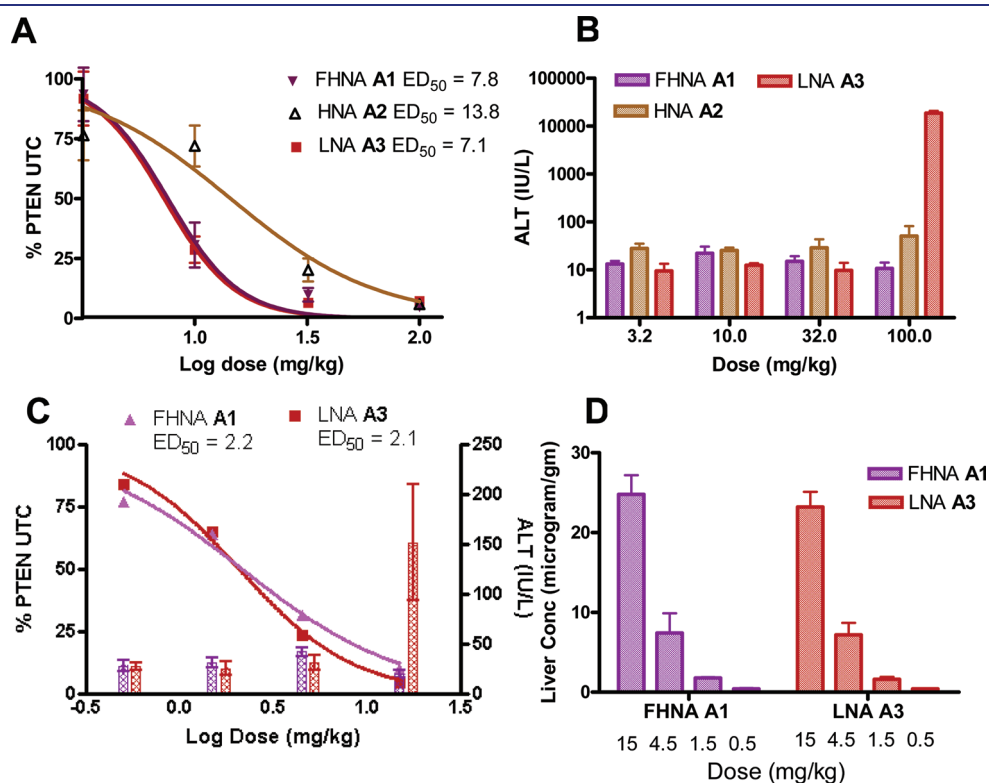


Figure 5. Biological evaluation of FHNA **A1**, HNA **A2**, and LNA **A3** ASOs in mice. (A) Mice ($n = 4$ /dose group) were injected i.p. with a single dose of 3.2, 10, 32, and 100 mg/kg of ASO in *saline*, and animals were sacrificed 72 h after the last dose. Liver PTEN mRNA was measured using quantitative RT-PCR. (B) Plasma ALT levels after sacrifice. (C) Mice ($n = 4$ /dose group) were injected i.p. twice a week for three weeks with 0.5, 1.5, 4.5, and 15 mg/kg of FHNA **A1** and LNA **A3** ASOs in *saline*, and animals were sacrificed 72 h after the last dose. Liver PTEN mRNA was measured using quantitative RT-PCR, and plasma ALT levels were recorded postsacrifice. (D) Tissue levels of FHNA and LNA ASOs from 3-week study.

FHNA A1 and LNA A3 ASOs in a three week study to investigate the effect on potency and toxicity in a subchronic dosing schedule. Mice were injected i.p. with 0.5, 1.5, 4.5, and 15 mg/kg of each ASO, and liver PTEN mRNA and plasma ALT levels were measured postsacrifice. Once again, the FHNA ASO A1 ($ED_{50} = 2.2$ mg/kg) exhibited identical potency as LNA ASO A3 ($ED_{50} = 2.1$ mg/kg). However, the high dose group LNA ASO A3 treated animals showed an increase in ALT levels but the FHNA ASOs did not show increased ALT levels at all the doses evaluated (Figure 5C). As in the case of the single dose study, we measured the tissue levels of FHNA ASO A1 and LNA ASO A3 in mouse liver but did not observe any meaningful differences in accumulation (Figure 5D).

DISCUSSION

Our biophysical and structural characterization of the FHNA and Ara-FHNA modifications reveals properties that are distinct from those of the corresponding fluoro-modified analogs of DNA, FRNA, and FANA. FHNA compares favorably with HNA in terms of RNA affinity, whereas Ara-FHNA causes a stability loss relative to HNA, FANA, and DNA that appears to be sequence dependent. Crystal structures at high resolution provide a qualitative rationalization of the thermodynamic data and reveal that the equatorial 3'-fluorine substituent in Ara-FHNA pushes away the 3'-flanking nucleotide, thus disrupting stacking of nucleobases. Evaluation of FHNA-modified ASOs in animal experiments revealed that these ASOs show comparable potency to LNA without producing hepatotoxicity. The excellent *in vivo* activity was obtained without the aid of complicated cationic lipids based formulations to deliver the ASO and is comparable to that observed with chemically modified and formulated siRNAs disclosed recently.³¹ Interestingly, while both FHNA and HNA modified ASOs showed similar activity in cell culture, the improved activity seen with FHNA in animal experiments suggests a positive role of fluorination for improving ASO uptake into tissues for therapeutic applications, an area of high interest.

The *in vivo* activity seen with the FHNA ASO was even more impressive considering that this modification showed considerably reduced duplex thermostability relative to LNA in the T_m studies. The rationale for the improved potency in animals is not clear and does not appear to be a result of increased biodistribution to liver or improved ASO metabolic stability. The pathways by which ASOs traverse cell membranes and navigate their way through the complex cellular milieu en route to their biological receptor (mRNA) are not well understood. However, it is known that chemically modified single stranded ASOs interact with cellular proteins and some of these interactions might be responsible for differential trafficking of ASOs to various sub-cellular compartments resulting in different pharmacological and toxicological properties.³² Nonetheless, our data support more aggressive evaluation of fluorinated oligonucleotides for therapeutic applications. Further studies aimed at investigating FHNA in other antisense mechanisms such as siRNA, miRNA, and splice modulation are underway and will be reported in due course. In conclusion, our data establish FHNA as a useful modification for antisense therapeutics and also confirm the stabilizing influence of $F(Py) \cdots H-C(Pu)$ pseudo hydrogen bonds in nucleic acid structures.

ASSOCIATED CONTENT

S Supporting Information. 1H , ^{13}C , and ^{19}F NMR spectra and analytical data for all new compounds; ^{31}P NMR spectra for all phosphoramidites; analytical data for oligonucleotides and dose response curves for cell culture experiments are provided. Atomic coordinates and structure factor data for the three crystal structures have been deposited in the Protein Data Bank (<http://www.rcsb.org>; 3Q61, FHNA-modified decamer and 3SD8, Ara-FHNA-modified decamer). This material is available free of charge via the Internet at <http://pubs.acs.org>.

AUTHOR INFORMATION

Corresponding Author

martin.egli@vanderbilt.edu; pseth@isisph.com

Present Addresses

[§]Regulus Therapeutics, 3545 John Hopkins Ct., San Diego, California 92121, United States

ACKNOWLEDGMENT

We thank Dr. Karsten Schmidt for HRMS measurements and Ms. Merry Daniel for help with the crystallization experiments. This work was supported in part by NIH Grant R01 GM55237 (to M.E.). Vanderbilt University is a member institution of LSCAT at the Advanced Photon Source (Argonne, IL). Use of the APS was supported by the U.S. Department of Energy, Basic Energy Sciences, Office of Science, under Contract No. W-31-109-Eng-38.

REFERENCES

- (1) Bennett, C. F.; Swayze, E. E. *Annu. Rev. Pharmacol. Toxicol.* **2010**, *50*, 259–293.
- (2) Valencia-Sanchez, M. A.; Liu, J.; Hannon, G. J.; Parker, R. *Genes Dev.* **2006**, *20*, 515–524.
- (3) Mattick, J. S. *PLoS Genet.* **2009**, *5*, e1000459.
- (4) Raal, F. J.; Santos, R. D.; Blom, D. J.; Marais, A. D.; Charng, M. J.; Cromwell, W. C.; Lachmann, R. H.; Gaudet, D.; Tan, J. L.; Chasan-Taber, S.; Tribble, D. L.; Flaim, J. D.; Crooke, S. T. *Lancet* **2010**, *375*, 998–1006.
- (5) Seth, P. P.; Siwkowski, A.; Allerson, C. R.; Vasquez, G.; Lee, S.; Prakash, T. P.; Wancewicz, E. V.; Witchell, D.; Swayze, E. E. *J. Med. Chem.* **2009**, *52*, 10–13.
- (6) Seth, P. P.; Allerson, C. R.; Berdeja, A.; Siwkowski, A.; Pallan, P. S.; Gaus, H.; Prakash, T. P.; Watt, A. T.; Egli, M.; Swayze, E. E. *J. Am. Chem. Soc.* **2010**, *132*, 14942–14950.
- (7) Seth, P. P.; Allerson, C. R.; Siwkowski, A.; Vasquez, G.; Berdeja, A.; Migawa, M. T.; Gaus, H.; Prakash, T. P.; Bhat, B.; Swayze, E. E. *J. Med. Chem.* **2010**, *53*, 8309–8318.
- (8) Prakash, T. P.; Siwkowski, A.; Allerson, C. R.; Migawa, M. T.; Lee, S.; Gaus, H. J.; Black, C.; Seth, P. P.; Swayze, E. E.; Bhat, B. *J. Med. Chem.* **2010**, *53*, 1636–1650.
- (9) Herdewijn, P. *Chem. Biodiversity* **2010**, *7*, 1–59.
- (10) Allerson, C. R.; Sioufi, N.; Jarres, R.; Prakash, T. P.; Naik, N.; Berdeja, A.; Wanders, L.; Griffey, R. H.; Swayze, E. E.; Bhat, B. *J. Med. Chem.* **2005**, *48*, 901–904.
- (11) Pallan, P. S.; Greene, E. M.; Jicman, P. A.; Pandey, R. K.; Manoharan, M.; Rozners, E.; Egli, M. *Nucleic Acids Res.* **2011**, *39*, 3482–3495.
- (12) Davis, S.; Propp, S.; Freier, S. M.; Jones, L. E.; Serra, M. J.; Kinberger, G.; Bhat, B.; Swayze, E. E.; Bennett, C. F.; Esau, C. *Nucleic Acids Res.* **2009**, *37*, 70–77.
- (13) Ng, E. W.; Shima, D. T.; Calias, P.; Cunningham, E. T., Jr; Guyer, D. R.; Adamis, A. P. *Nat. Rev. Drug Discovery* **2006**, *5*, 123–132.

- (14) Hagmann, W. K. *J. Med. Chem.* **2008**, *51*, 4359–4369.
- (15) Damha, M. J.; Wilds, C. J.; Noronha, A.; Brukner, I.; Borkow, G.; Arion, D.; Parniak, M. A. *J. Am. Chem. Soc.* **1998**, *120*, 12976–12977.
- (16) Abramov, M.; Marchand, A.; Calleja-Marchand, A.; Herdewijn, P. *Nucleosides, Nucleotides Nucleic Acids* **2004**, *23*, 439–455.
- (17) Allart, B.; Busson, R.; Rozenski, J.; Van Aerschot, A.; Herdewijn, P. *Tetrahedron* **1999**, *55*, 6527–6546.
- (18) Pérez-Pérez, M.-J.; De Clercq, E.; Herdewijn, P. *Bioorg. Med. Chem. Lett.* **1996**, *6*, 1457–1460.
- (19) Bennua-Skalmowski, B.; Vorbrüggen, H. *Tetrahedron Lett.* **1995**, *36*, 2611–2614.
- (20) Takamatsu, S.; Katayama, S.; Hirose, N.; De Cock, E.; Schelkens, G.; Demillequand, M.; Brepoels, J.; Izawa, K. *Nucleosides, Nucleotides Nucleic Acids* **2002**, *21*, 849–861.
- (21) Kim, D. W.; Ahn, D.-S.; Oh, Y.-H.; Lee, S.; Kil, H. S.; Oh, S. J.; Lee, S. J.; Kim, J. S.; Ryu, J. S.; Moon, D. H.; Chi, D. Y. *J. Am. Chem. Soc.* **2006**, *128*, 16394–16397.
- (22) Foster, A. B.; Hems, R.; Webber, J. M. *Carbohydr. Res.* **1967**, *5*, 292–301.
- (23) Manta, S.; Tzioumaki, N.; Tsoukala, E.; Panagiotopoulou, A.; Pelecanou, M.; Balzarini, J.; Komiotis, D. *Eur. J. Med. Chem.* **2009**, *44*, 4764–4771.
- (24) Verheggen, I.; Van Aerschot, A.; Toppet, S.; Snoeck, R.; Janssen, G.; Balzarini, J.; De Clercq, E.; Herdewijn, P. *J. Med. Chem.* **1993**, *36*, 2033–2040.
- (25) Seth, P. P.; Vasquez, G.; Allerson, C. A.; Berdeja, A.; Gaus, H.; Kinberger, G. A.; Prakash, T. P.; Migawa, M. T.; Bhat, B.; Swayze, E. E. *J. Org. Chem.* **2010**, *75*, 1569–1581.
- (26) Anzahaee, M. Y.; Watts, J. K.; Alla, N. R.; Nicholson, A. W.; Damha, M. J. *J. Am. Chem. Soc.* **2011**, *133*, 728–731.
- (27) Froeyen, M.; Wroblowski, B.; Esnouf, R.; De Winter, H.; Allart, B.; Lescrinier, E.; Herdewijn, P. *Helv. Chim. Acta* **2000**, *83*, 2153–2182.
- (28) Lavery, R.; Sklenar, H. *J. Biomol. Struct. Dyn.* **1989**, *6*, 655–667.
- (29) Li, F.; Sarkhel, S.; Wilds, C. J.; Wawrzak, Z.; Prakash, T. P.; Manoharan, M.; Egli, M. *Biochemistry* **2006**, *45*, 4141–4152.
- (30) Freier, S. M.; Alkema, D.; Sinclair, A.; Neilson, T.; Turner, D. H. *Biochemistry* **1985**, *24*, 4533–4539.
- (31) Manoharan, M.; Akinc, A.; Pandey, R. K.; Qin, J.; Hadwiger, P.; John, M.; Mills, K.; Charisse, K.; Maier, M. A.; Nechev, L.; Greene, E. M.; Pallan, P. S.; Rozners, E.; Rajeev, K. G.; Egli, M. *Angew. Chem., Int. Ed.* **2011**, *50*, 2284–2288.
- (32) Koller, E.; Vincent, T. M.; Chappell, A.; De, S.; Manoharan, M.; Bennett, C. F. *Nucleic Acids Res.* **2011**, *39*, 4795–4807.